The Journal of Membrane Biology (2020) 253:287–298
https://doi.org/10.1007/s00232-020-00124-3

Experimental and Computational Characterization of Oxidized and Reduced Protegrin Pores in Lipid Bilayers

Mykola V. Rodnin[1] · Victor Vasquez-Montes[1] · Binod Nepal[2] · Alexey S. Ladokhin[1] · Themis Lazaridis[2,3]

Received: 23 March 2020 / Accepted: 23 May 2020 / Published online: 4 June 2020

Abstract

Protegrin-1 (PG-1), an 18-residue β-hairpin stabilized by two disulfide bonds, is a member of a family of powerful antimicrobial peptides which are believed to act through membrane permeabilization. Here we used a combination of experimental and computational approaches to characterize possible structural arrangements of PG-1 in lipid bilayers mimicking bacterial membranes. We have measured the dose–response function of the PG-1-induced leakage of markers of various sizes from vesicles and found it to be consistent with the formation of pores of two different sizes. The first one allows the release of small dyes and occurs at peptide:lipid ratios < 0.006. Above this ratio, larger pores are observed through which the smallest of dextrans FD4 can be released. In parallel with pore formation, we observe a general large-scale destabilization of vesicles which is probably related to complete rupture of some vesicles. The population of vesicles that are completely ruptured depends linearly on PG-1:lipid ratio. Neither pore size, nor vesicle rupture are influenced by the formation of disulfide bonds. Previous computational work on oxidized protegrin is complemented here by all-atom MD simulations of PG-1 with reduced disulfide bonds both in solution (monomer) and in a bilayer (dimer and octamer). The simulations provide molecular insights into the influence of disulfide bonds on peptide conformation, aggregation, and oligomeric structure.

Keywords Protegrin · Antimicrobial peptides · Fluorescence · Membranes · Molecular dynamics

Introduction

The protegrins are a family of five antimicrobial peptides isolated from porcine leukocytes (Kokryakov et al. 1993). They have 16–18 residues and a β-hairpin structure stabilized by two disulfide bonds (Aumelas et al. 1996; Fahrner et al. 1996; Usachev and Klochkova 2015; Usachev et al. 2017). The best-studied member of this family is protegrin-1 (PG-1), whose structure in biological membranes has been studied with neutron diffraction (Yang et al. 2000), oriented CD (Heller et al. 1998), solid-state NMR (Yamaguchi et al. 2002; Mani et al. 2006; Tang and Hong 2009), AFM (Lam et al. 2012; Henderson et al. 2016). The size of PG-1 pores was estimated to be below 21 Å in diameter, based on polyethylene glycol permeation assay (Mani et al. 2006). However, another study that investigated PG-1-induced dextran leakage suggested a pore diameter of at least 3–4 nm at high salt concentrations (Lai et al. 2006). Investigations of the effect of disulfide bonds on antimicrobial activity and membrane translocation produced seemingly conflicting results (Harwig et al. 1996; Mangoni et al. 1996; Lai et al. 2002; Dawson and Liu 2010).

Computational studies of PG-1 have also been extensive (Bolintineanu and Kaznessis 2011; Lipkin and Lazaridis 2017a), including both implicit solvent (Rui and Im 2010; Lazaridis et al. 2013; Lipkin and Lazaridis 2015, 2017b) and all-atom simulations (Jang et al. 2006; Langham et al. 2008; Rui et al. 2009; Vivcharuk and Kaznessis 2010; Prieto et al. 2014). Recent work involved very long all-atom simulations of various oligomers in different arrangements in POPC and POPG membranes (Lipkin et al. 2017). It was

✉ Alexey S. Ladokhin
aladokhin@kumc.edu

✉ Themis Lazaridis
tlazaridis@ccny.cuny.edu

[1] Department of Biochemistry and Molecular Biology, The University of Kansas Medical Center, Kansas City, KS 66160, USA

[2] Department of Chemistry and Biochemistry, City College of New York, New York, NY 10031, USA

[3] Graduate Programs in Chemistry, Biochemistry, and Physics, The Graduate Center, City University of New York, New York, NY 10016, USA

found that unsheared beta barrels were unstable. Sheared barrels appeared stable on the 10-μs timescale, although formation of such barrels starting from monomers, dimers, or tetramers was not observed on that timescale. In addition, alternative structures with partially associated peptides were also observed preventing a firm conclusion on the structure of the pores.

Despite the large amount of work on protegrins, the structure and the size of the pores it makes in lipid bilayers remains uncertain. Here we perform a series of experiments of PG-1 interacting with lipid bilayer vesicles. The experiments provide information on the affinity of the peptide for vesicles of different charge, the cooperativity of membrane binding, and the size of the pores the peptide forms in lipid bilayers. The pore sizing experiments are based on the release of markers of different sizes, a technique previously used to study pores of various host defense peptides (Wimley et al. 1994; Ladokhin et al. 1997). Based on the experimental finding that disulfide reduction has no appreciable effect on membrane binding or pore formation, we repeat some of the previous atomistic simulations in the absence of the disulfide bonds and obtain a molecular rationalization of the experimental findings.

Materials and Methods

Materials

Palmitoyl-oleoyl-phosphatidylcholine (POPC) and palmitoyl-oleoyl-phosphatidylglycerol (POPG) were purchased from Avanti Polar Lipids (Alabaster, AL). The fluorescent dyes ANTS and DPX were obtained from Invitrogen (Carlsbad, CA), while fluorescein and the fluorescein-labeled dextrans were purchased from Sigma (St. Louis, MO). Fluorescence studies employed a wild-type variant of protegrin PG-1 (RGGRLCYCRRRFCVCVGR-NH2) labeled at the N-terminus with the fluorescent dye nitrobenzoxadiazole (NBD) and a variant with a Phe to Trp substitution at position 12 (RGGRLCYCRRRWCVCVGR-NH2). The peptides were purchased from New England Peptides at 95% purity and Peptide 2.0 Inc. at 98% purity, respectively.

Preparation of Large Unilamellar Vesicles (LUV)

Mixtures of POPC and POPG in chloroform were dried under the flux of nitrogen and then dried overnight under high vacuum. The phospholipid film was suspended in 50 mM Tris–HCl buffer, pH 8.0 and extruded 10 times through 100 nm Nucleopore polycarbonate membranes (Millipore, St Louis, MO). In the case of LUV loaded with fluorophores, the resuspended lipid mixture in buffer was mixed with the desired probes prior to extrusion followed by freeze thaw cycles in liquid nitrogen (after each extrusion). The fluorescent probes were added at the following concentrations: fluorescein (FL) and the fluorinated dextran FD4 at 2 mg/mL, FD20 to FD70 at 4 mg/mL and ANTS/DPX at 10/50 mM. Loaded vesicles were isolated from non-included components by size-exclusion chromatography on a 1 × 30 cm Superose 6 column.

Pore-Sizing Experiments

The leakage of LUV (1.0 mM) preloaded with fluorescent dextrans (FD) was initiated by mixing the solution with 3, 6, 9, 12 or 20 μM of PG-1 (120 μL total volume). The sample was incubated for 30 min at room temperature and the leakage of fluorescent compounds was strongly reduced by introducing a 5 × excess of empty LUV (without incorporated fluorophores). All the reactions were conducted in 50 mM Tris–HCl buffer, pH 8.0. The final mixtures were subjected to size-exclusion chromatography using an AKTA FPLC Purifier, on a 1 × 30 cm Superose 6 column, at a flow rate of 0.3 mL/min. Absorbance was recorded at 492 nm. The peak areas corresponding to LUV and free dyes were calculated using Unicorn 5.10 software. Since the molar absorption of fluorinated dextrans used in this study (FD4, 20, 40 and 70) and fluorescein at the same w/v concentration are different, we used 2 mg/mL concentration for fluorescein and FD4 and 4 mg/mL for FD20, 40, and 70. This allowed us to have approximately equal peak area for different compounds. Calibration of 1 × 30 cm Superose 6 column enabled us to determine the retention volumes for the compounds used here: for LUV, fluorescein, FD4, FD20, FD40 , and FD70 they were 8, 20, 18, 17.5, 16.5, and 14 mL, respectively. To establish "zero leakage" we used LUV without PG-1 addition, while "100% leakage" was determined after fully dissolving the LUV with Triton X-100. Non-specific absorption signals that arise from non-specific leakage (due to storage) and from empty LUV at 492 nm were subtracted from the calculated peak area.

Spectroscopic Measurements

The leakage of ANTS/DPX loaded vesicles was conducted in 50 mM Tris–HCl buffer, pH 8.0, at room temperature. Samples were prepared in a 400 μL total volume in the presence or absence of 1.0 mM 2-mercaptoethanol (ME) to compare the activity of native and reduced PG-1. NBD fluorescence measurements employed 2.0 μM PG-1 N-terminally labeled with NBD and varying concentrations of 25POPG:75POPC LUV in 50 mM Tris–HCl buffer, pH 8.0. Fluorescence was recorded on SPEX Fluorolog FL3-22 steady-state fluorescence spectrometer (Jobin Yvon, Edison, NJ) equipped with double-grating excitation and emission monochromators. Measurements were performed in a

2 × 10 mm cuvette oriented perpendicular to the excitation beam. For the kinetic recording of ANTS/DPX release, we used the following settings: excitation 353 nm, emission 520 nm, excitation/emission slits 2/14, respectively. The reaction was stopped by the addition of 20 µL 20% Triton X-100. NBD measurements were collected from 480 to 650 nm using an excitation wavelength of 470 nm and 5 nm slits for both emission and excitation.

Membrane Partitioning Calculations

The association of PG-1 to lipid bilayers is indicated by the increase in NBD intensity (measured at a constant wavelength) as a function of LUV concentration. The data were plotted as the relative intensity increase (I) against experimental lipid concentration ([L]) and fitted to the following equation (White et al. 1998):

$$I = 1 + (I_{\infty} - 1)\left(\frac{K_x \cdot [\mathrm{L}]}{[\mathrm{W}] + (K_x \cdot [\mathrm{L}])}\right) \tag{1a}$$

where I_{∞} is the intensity at an infinite lipid saturation, [W] is the concentration of water (55.3 M) and K_x denotes the mole fraction partitioning coefficient, defined as:

$$K_x = \frac{[\mathrm{P_{bil}}]/[L]}{[\mathrm{P_{water}}]/[\mathrm{W}]} \tag{1b}$$

where $[\mathrm{P_{water}}]$ and $[\mathrm{P_{bil}}]$ represent the bulk concentrations of PG-1 in water and associated to the bilayer. The calculated partitioning constant (K_x) was used to determine membrane partitioning free energy (ΔG) using the following formula:

$$\Delta G = -RT \cdot \ln(K_x) \tag{2}$$

where R is the gas constant (1.985×10^{-3} kcal/Kmol) and T is the experimental temperature in Kelvin (298 K).

Molecular Dynamics Simulations

The initial structure for the solution simulation was downloaded from the Protein Data Bank (PDB ID 1PG1) (Fahrner et al. 1996). The initial structures for the dimer and octameric sheared barrel were taken from previous simulations (Lipkin et al. 2017). The structures were edited to remove the disulfide bond and add a hydrogen atom to the sulfur atom of each CYS residue. The structures were minimized and equilibrated again with NAMD 2.11 (Phillips et al. 2005) using the CHARMM c36 force field (Huang and Mackerell 2013). The production simulation runs were carried out on the Anton 2 supercomputer (Shaw et al. 2014) at the Pittsburgh Supercomputing Center with a 2.5 fs time step. The simulations of monomer in aqueous solution, dimer on the membrane surface, and octameric barrel embedded in the membrane were carried out for 1, 3, and 5 µs, respectively. Membranes were composed of 75% POPC + 25% POPG and the system contained 0.15 M KCl. The coordinates were saved every 1 ns. Nonbonded interaction cutoff values were automatically selected by the Anton software. Temperature was maintained at 310 K using the Nose–Hoover thermostat.

Experimental Results

Partitioning of PG-1 to Anionic Bilayers

The propensity of PG-1 to interact with membranes was examined using a PG-1 variant conjugated to the environmentally sensitive probe NBD at its N-terminus. Fluorescence measurements were collected at progressively higher [LUV] (large unilamellar vesicles) containing the anionic lipid phosphatidylglycerol (POPG) in a phosphatidylcholine (POPC) matrix.

The incremental addition of 25POPG:75POPC LUV to a PG-1 containing solution led to large concentration-dependent increase in fluorescence maximum (Fig. 1a). These were accompanied by a shift in the position of the maximum from 546 nm in solution to 535 nm at 1.5 mM LUV. Together with the increase in intensity, the spectral blue shifts are characteristic of NBD transitioning to hydrophobic environments and indicate the partitioning of PG-1 to the bilayer. The partitioning of PG-1 was dependent on the anionic content of the bilayers. Measurements performed in the presence of zwitterionic POPC LUV did not produce changes in NBD intensity (Fig. 1b, black), attributed to lack of binding to zwitterionic membranes. Increasingly stronger binding was observed as a function of the anionic lipid POPG (Fig. 1b). The results obtained with 25POPG:75POPC LUV were fitted to Eq. 1 to obtain the membrane partitioning constant K_x. These values were then employed to calculate the membrane partitioning free energy (ΔG) using Eq. 2, yielding a $\Delta G = -7.8 \pm 0.1$ kcal/mol. The results obtained with bilayers containing 10% POPG (Fig. 1b, yellow) and 50% POPG (Fig. 1b, green) could not be accurately fitted to obtain reliable ΔG values.

Measurements were repeated with 25POPG:75POPC LUV pre-incubated with a tenfold excess of unlabeled PG-1 (3 µM peptide). The interaction of 0.3 µM labeled PG-1 with these pre-incubated LUV had $\Delta G = -8.5 \pm 0.1$ kcal/mol (Fig. 1c, red), lower by 0.7 kcal/mol than the value obtained for 25POPG:75POPC LUV experiments in the absence of pre-incubated PG-1 (Fig. 1c, blue). The uncertainty in the ΔG values was calculated by support-plane analysis (Montgomery and Peck 1982) (Fig. 1d). This gain in ΔG suggests that the interaction of PG-1 with the membrane is cooperative.

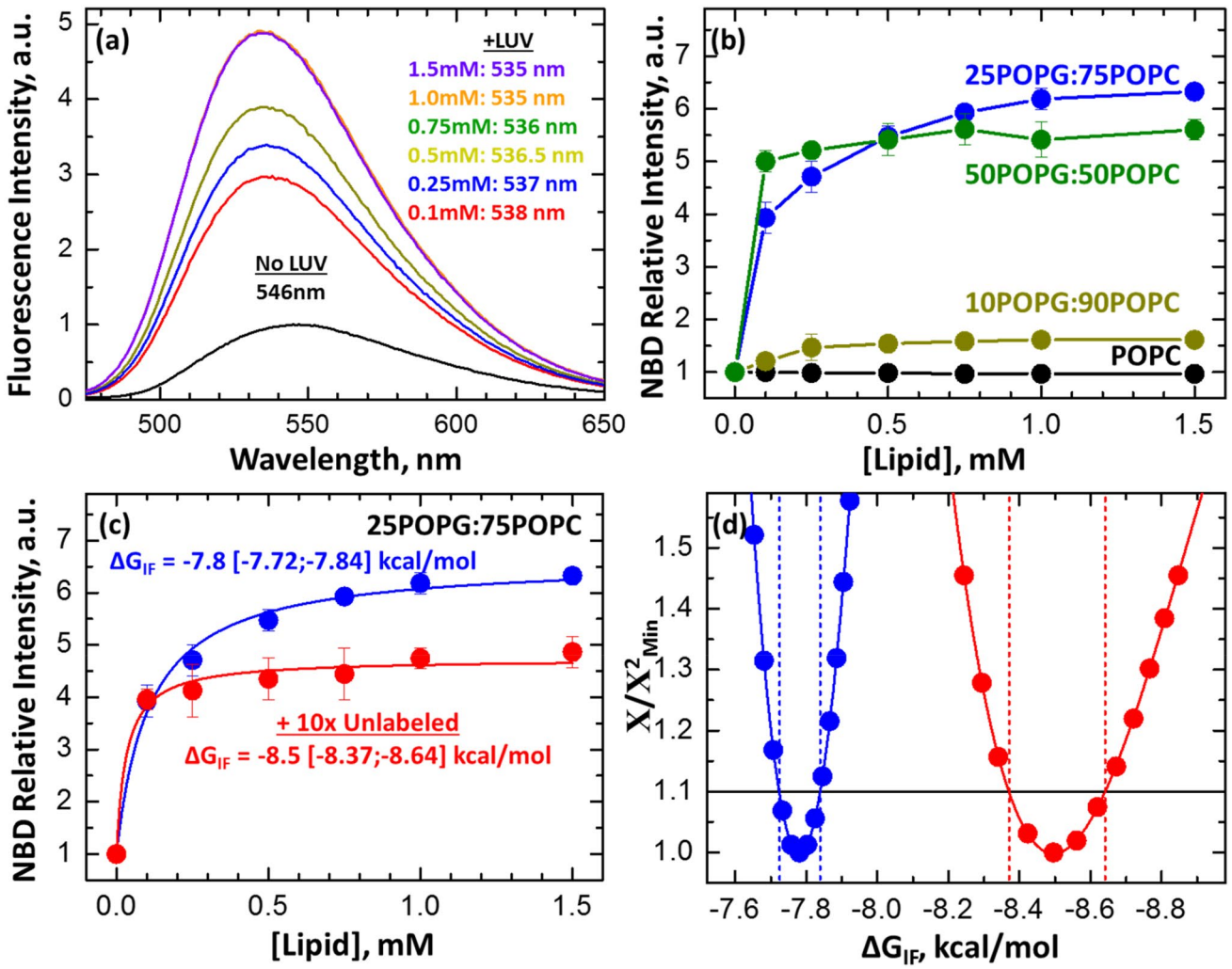

Fig. 1 PG-1 membrane partitioning. **a** The interaction of NBD-labeled PG-1 with anionic 25POPG:75POPC LUV was detected by increases in intensity and blue shifts of the NBD fluorophore as a function of lipid concentration. **b** The interaction of PG-1 with membranes is lipid dependent and requires at least 25% of anionic lipid POPG. (Note that in 50% POPG, the binding is virtually complete at the lowest lipid concentration, therefore this composition was used in further leakage studies). **c** Quantitative analysis of membrane partitioning of NBD-labeled PG-1 into 25POPG:75POPC vesicles (blue) indicates a large free energy of partitioning of − 7.8 kcal/mol (solid line obtained using Eqs. 1–2). The free energy is further increased to − 8.5 kcal/mol when the membranes were loaded with unlabeled PG-1 (red), suggesting that membrane binding of PG-1 is cooperative. **d** The robustness of the fits was estimated using support-plane analysis. The calculated error range (vertical lines) is indicated in brackets. The horizontal line represents 1-standard deviation from the lowest X/X^2_{Min} fit. The values below this threshold are defined as indistinguishable fits (Color figure online)

PG-1 Induced Membrane Leakage and Pore Formation

The ability of PG-1 to induce membrane leakage was measured in anionic LUV composed of 50POPG:50POPC encapsulating the fluorophore ANTS and its quencher DPX. Measurements were performed using a PG-1 variant with a F12W substitution introduced to facilitate the calculation of accurate peptide concentrations. This variant exhibits the same cytotoxicity as the original peptide (Drin and Temsamani 2002).

Kinetic measurements showed fast permeabilization in the presence of 1:200 peptide:lipid ratio that saturated at 60% leakage after ~ 1 min (Fig. 2). The leakage of LUV was detected by the increase in fluorescence intensity of the ANTS fluorophore that is detected due to the release of the encapsulated contents and the dilution of its quencher DPX. Measurements at 1:500 peptide:lipid ratio showed significantly lower leakage that only achieved 10% release after 15 min. The influence of the two disulfide bonds present in PG-1 on this process was characterized by performing leakage measurements in the presence or absence of 1.0 mM of

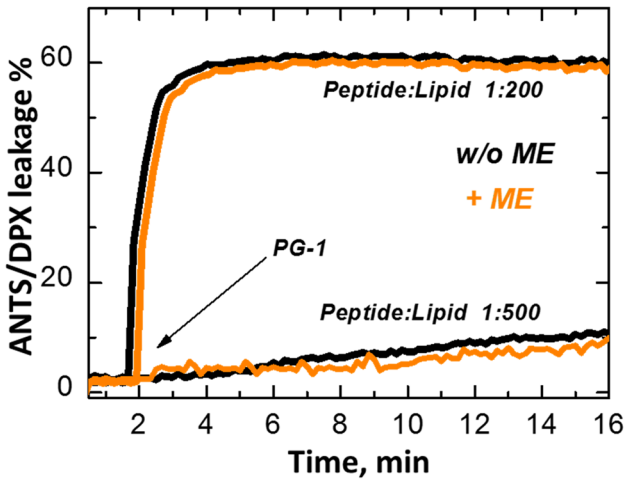

Fig. 2 PG-1 induced leakage of anionic bilayers. The leakage of ANTS/DPX probes encapsulated in 50POPG:50POPC LUV was measured before and after the addition of PG-1. The kinetics of the leakage event were dependent on [peptide], with samples containing 1:200 peptide:lipid ratios showing a fast saturation at ~ 60% leakage. The reduced state of the peptide, controlled by the addition of 2-mercapthoethanol (ME) indicated in orange, did not affect leakage kinetics (Color figure online)

the reducing agent 2-mercaptoethanol (ME). The addition of ME had no effect on the leakage kinetics, suggesting that the membrane leakage caused by PG-1 is not affected by the oxidation state of its disulfide bonds. Control measurements showed that ME by itself did not cause leakage of the compounds from LUV.

To establish size of the pores formed by PG-1, we performed leakage measurements on LUV with encapsulated fluorescent probes of different sizes. LUV composed of 50POPG:50POPC and preloaded with either free fluorescein dye (Fl) or Fl-labeled dextrans were incubated with various concentrations of [PG-1]. The samples were subsequently run through a gel filtration column to determine the amount of released material with the results presented in Fig. 3. The release of the smallest marker, Fl, is observed at low peptide-to-lipid ratio of P/L = 0.003 and reaches completion by P/L = 0.02. The release of larger dextrans (FD20, FD40 and FD70) increases linearly with protegrin concentration and is insensitive to the size of the dextran. This is indicative of either very large pores, or, more likely, of the collapse of a subpopulation of the vesicles resulting in a complete release of their contents. Interestingly, the release of the smallest dextran, FD4, starts similarly to the non-discriminate release of larger dextrans, but then increases sharply and reaches that for the level of smaller Fl at P/L ~ 0.012. This pattern is indicative of the formation of a pore that can allow the leakage of FD4, but not that of a larger dextran at L/P above 0.06. The size of the pore at P/L below 0.06 is smaller, allowing the release of Fl, but not of FD4. Similarly to the ANTS/DPX leakage measurements (Fig. 2), the addition of ME had no effect on the size of the two pores capable of releasing Fl (Fig. 3b, black) or FD4 (Fig. 3b, red).

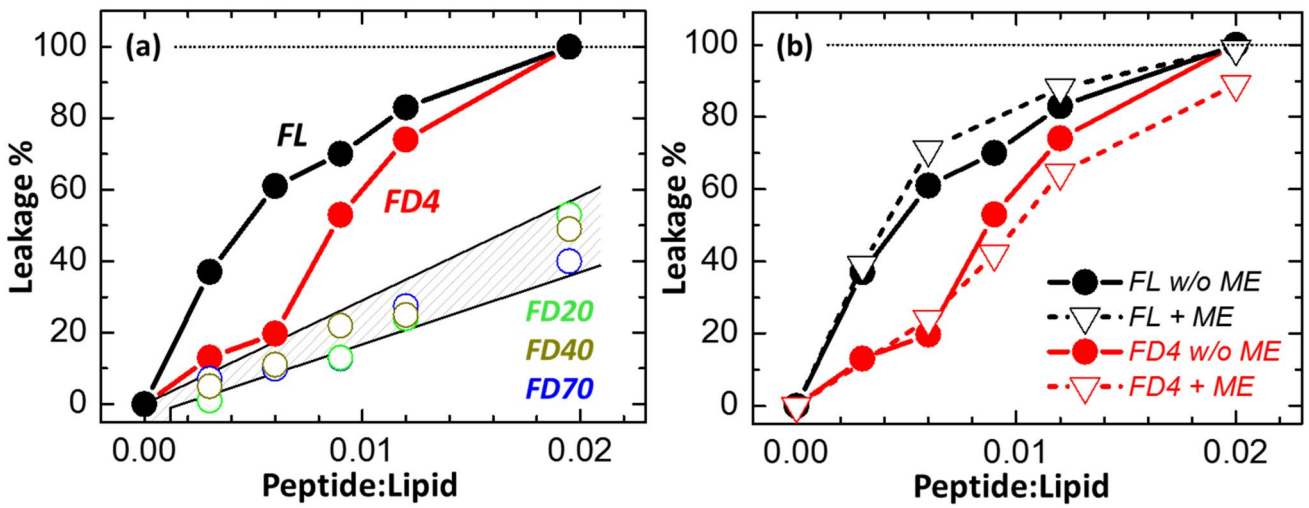

Fig. 3 Sizing of PG-1 pores in anionic 50POPG:50POPC membranes. Leakage experiments on LUV loaded with fluorescent probes of varying sizes. The results are indicated as the peptide:lipid ratio in the sample and analyzed assuming the membrane binding of all peptide molecules present. **a** The largest response was observed for fluorescein (FL) and the fluorescent dextran (FD) FD4 (maximal leakage possible is indicated by horizontal lines). Significantly lower leakage was observed for FD20 and larger probes. The linear leakage observed for the larger FD probes is attributed to non-specific leakage, likely due to membrane destabilization. **b** The leakage of both fluorescein and FD4 was not affected by the addition of 2-mercaptoethanol (ME). This suggests that the oxidation state of the PG-1 disulfide bonds does not have a substantial effect on pore size (Color figure online)

Computational Results

The observation that reduction of the disulfide bonds did not produce a substantial change in leakage and pore size prompted us to examine the effect of disulfide bonds computationally. We previously performed multimicrosecond simulations of various oligomeric constructs of PG-1 with intact disulfide bonds either on the membrane surface or embedded into the membrane (Lipkin et al. 2017). It was found that the NCNC dimer was most stable on the membrane surface and a sheared octameric barrel was most stable in the membrane. Here we repeat these two simulations in the absence of disulfide bonds. We also add a simulation of the monomer in aqueous solution, also in the absence of disulfide bonds, to gauge the intrinsic propensity of the monomer toward the β-hairpin structure. Table 1 lists the systems simulated.

Aqueous Phase Simulation of PG-1 Monomer

Without the disulfide bonds, the peptide completely unfolds after 50 ns and refolds after 150 ns. It then undergoes folding and unfolding multiple times, sampling different conformations. After 500 ns it attains a stable, folded conformation until the end of the 1-μs simulation. The final structure is also a β-hairpin but with different CO···NH hydrogen bonds between the beta strands (Fig. 4). Specifically, the initial equilibrated β-hairpin has H bonds between residues 9–12, 7–14, and 5–16. The refolded structure has H bonds between residues 8–12, 6–14, and 4–16 and the position of the turn has changed from residue 11 to residue 10. As a result of the refolding, Cys residues now are on both faces of the hairpin.

Table 1 Systems simulated by all-atom molecular dynamics

PG-1 system	Environment	Duration
Monomer	Solution	1 μs
NCNC dimer (parallel)	75% POPC + 25% POPG, on surface	5 μs
Sheared octameric β-barrel	75% POPC + 25% POPG, inserted	5 μs

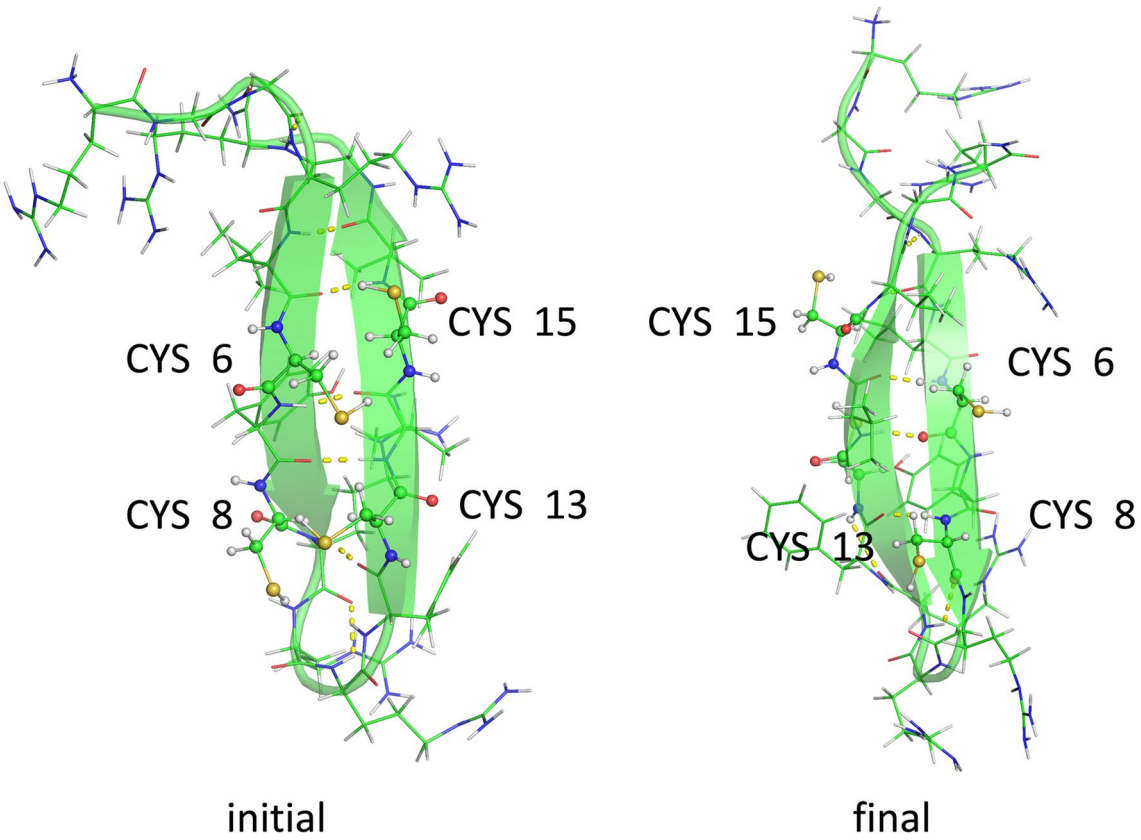

Fig. 4 Initial (left) and final (right) structures of the PG-1 monomer after 1 μs of simulation in aqueous solution (Color figure online)

Dimer on the Membrane Surface

The simulation of a parallel NCNC dimer (the C-terminal strand of one associated with the N-terminal strand of the other) on the bilayer surface started from a configuration equilibrated in previous work (Lipkin et al. 2017) but with the disulfide bonds removed. The dimer was stable throughout the 5-μs simulation and the monomers maintained their original H bonding pattern, unlike the monomer simulation in bulk water. This may be due to kinetic reasons or to the influence of the membrane. The top and side views of the final snapshot are shown on the right side of Fig. 5. The corresponding snapshots for the oxidized form, taken from previous work (Lipkin et al. 2017), are shown on the left side. Side view of Fig. 5 shows that in both systems hydrophobic residues LEU 5, TYR 7, PHE 12, VAL 14 and VAL 16 insert into the membrane and positively charged residues interact with the lipid head groups. As expected, the peptides tend to interact more with POPG head groups, which causes an increased concentration of POPG near the vicinity of the peptide. Membrane thickness calculations (Fig. 6) show some membrane thinning in the vicinity of the peptide.

The interaction energy between two monomers was -47.6 ± 16.2 kcal/mol, whereas the corresponding interaction energy with disulfide bonds present was -23.7 ± 17.4 kcal/mol. This interaction energy consists of electrostatic and van der Waals contributions. Further analysis shows that the difference is due to stronger backbone-backbone interactions in the reduced system (-40 ± 5 vs. -28 ± 5 kcal/mol, with the van der Waals energy being -5.5 kcal/mol in both cases). In corroboration, the 6 H bonds between the two monomers are shorter

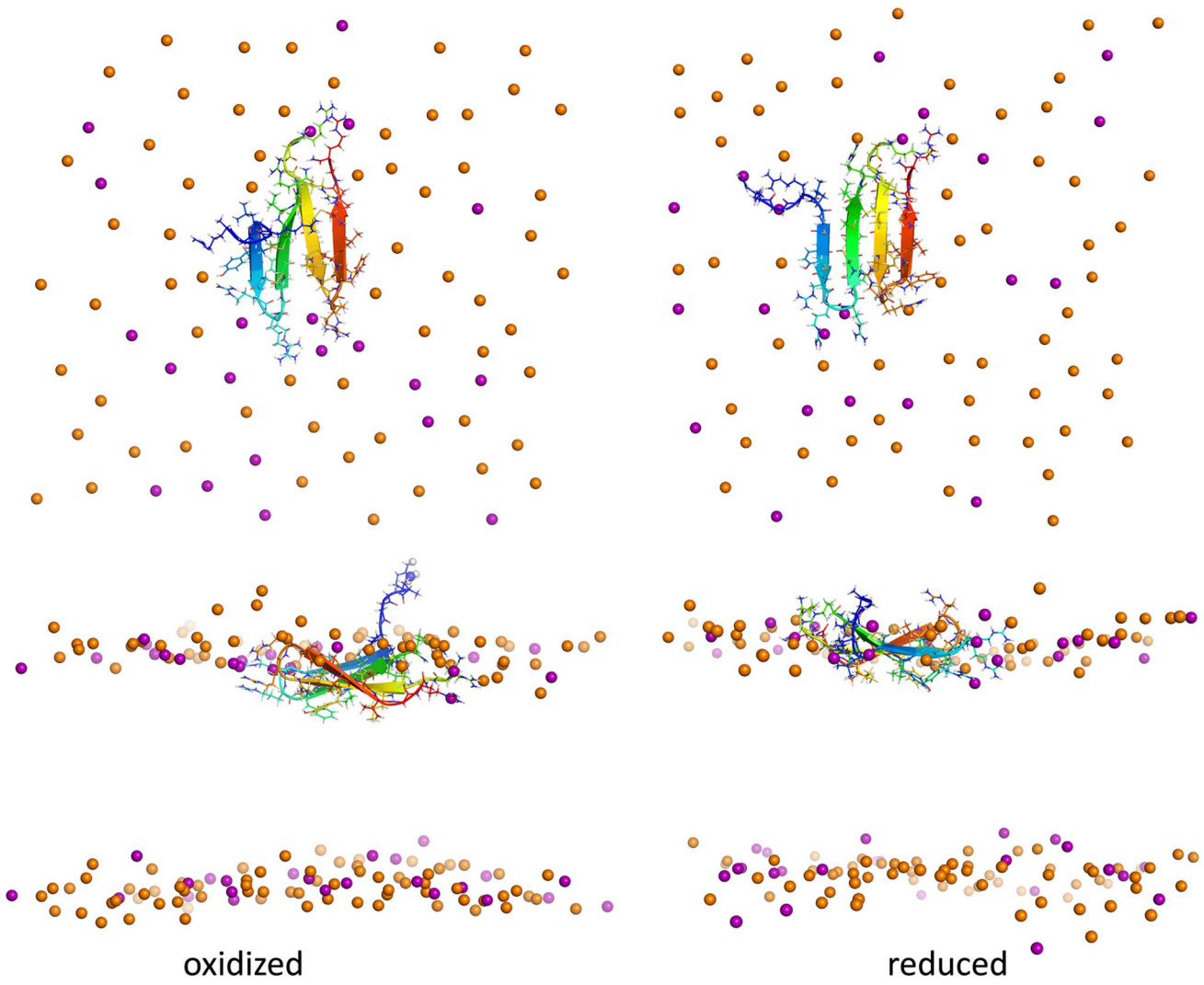

Fig. 5 Top and side views of the PG-1 dimer on the membrane surface after 5 μs simulation. Left, oxidized; Right, reduced. For clarity, only the lipid headgroups are shown (orange for POPC and purple for POPG) (Color figure online)

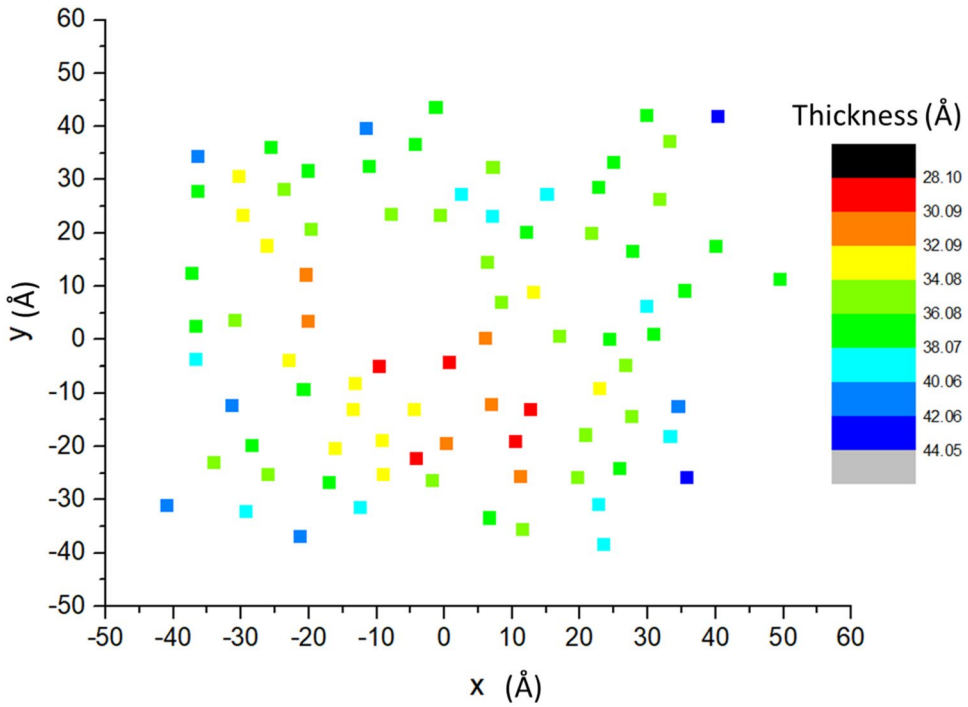

Fig. 6 Membrane thickness at different points on the membrane plane for parallel NCNC dimer on the membrane surface. Membrane thickness is calculated as phosphate to phosphate distance (Color figure online)

in the reduced form (2.3 ± 1.0 vs. 2.8 ± 1.4 Å). It seems that the disulfide bonds strain the hairpin backbone and prevent optimal interactions with a neighboring hairpin.

Octameric Sheared Barrel

Around 1.2 μs, one of the monomers starts to move towards the pore interior and this leads to an opening in the barrel. The opening is not very large and remains until 2.4 μs, when the barrel closes again but in a more sheared position. After that, there is no change until the end of the 5-μs simulation. The barrel is stable but more sheared than the initial barrel (Fig. 7). The pore radius over the last μs is 9.4 Å, somewhat larger than the 8.7 Å with disulfide bonds. The larger size of the pore may be due to an expansion in width of each beta hairpin due to the absence of disulfide bonds. The measured hydrogen bond distances within each beta hairpin indicate that in most cases there is an increase in intramolecular H-bond distance when the disulfide bonds are reduced (Table 2). This is in contrast to the shortening of the intermolecular H bonds seen in the dimer. Energy analysis shows that the reduction of the disulfide bonds increases the interactions of the SH groups with their neighbors (Table 3). Figure 7 also shows that POPG molecules tend to cluster around the peptide barrel, which is expected based on the high positive charge of the peptide.

Discussion and Conclusions

The main experimental findings in this work can be summarized as follows: (a) PG-1 has undetectable affinity for zwitterionic membranes; the affinity increases as the membrane negative charge increases and is − 7.8 kcal/mol for a 25:75 POPG/POPC membrane, (b) membrane binding is cooperative, i.e. it gets stronger as the peptide concentration in the membrane increases, (c) at low peptide concentrations (P/L < 0.006) PG-1 makes small pores that allow the passage of only small molecules such as fluorescein (8–10 Å diameter), (d) at moderate concentrations (P/L 0.009–0.012) PG-1 makes larger pores that allow the passage of molecules like FD4 (hydrodynamic radius 14 Å) but not FD20 (hydrodynamic radius 33 Å) or larger, (d) in parallel with pore formation, a large-scale destabilization of the vesicles, likely complete rupture, appears to be taking place at a low rate. The population of vesicles that are completely ruptured depends linearly on PG-1:lipid ratio. (e) Neither pore size, nor vesicle rupture are influenced by the formation of disulfide bonds.

It is worth comparing the present results to published reports. Lai et al. (Lai et al. 2006) measured a binding affinity of − 7 kcal/mol for PG-1 binding to 70:DOPC/30:DOPG vesicles using isothermal titration calorimetry (ITC). Another ITC study also found a free energy of − 7 kcal/mol for binding to 75:POPC/25:POPG

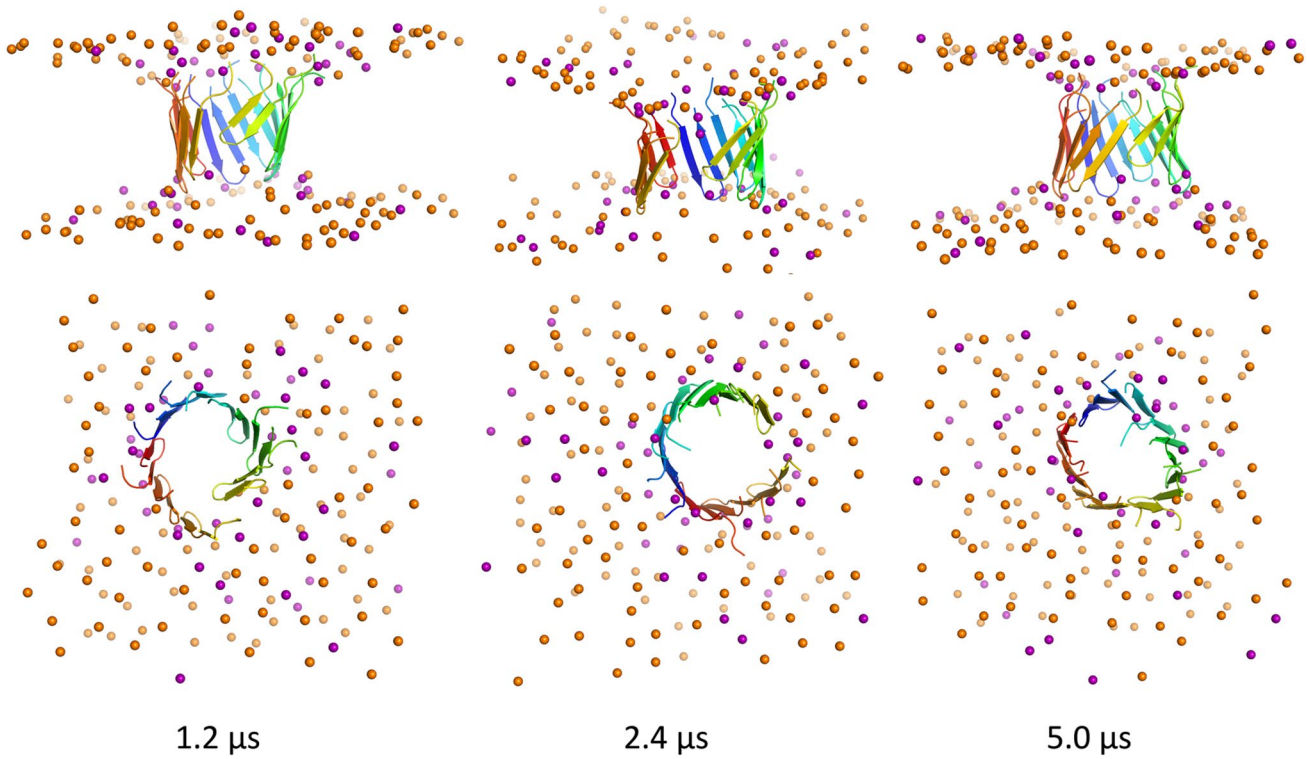

Fig. 7 Structure of sheared octameric β-barrel of PG-1 at different simulation times. For clarity, only the lipid headgroups are shown (orange for for POPC and purple for POPG) (Color figure online)

Table 2 Average intramolecular H-bond distances (Å) in each of the 8 PG-1 monomers in the barrel. The most prominent beta sheet H bonds are considered in the average, which include six NH···O hydrogen bonds between residues 5, 7, 9, 12, 14, and 16

w/o disulfide bonds								
Average	2.11	2.15	2.07	3.20	2.18	2.10	2.14	2.11
SD	0.36	0.57	0.30	1.94	0.58	0.39	0.38	0.36
With disulfide bonds								
Average	2.07	2.17	2.11	2.17	2.09	2.13	2.13	2.07
SD	0.35	0.63	0.34	0.47	0.42	0.53	0.40	0.35

Table 3 Interaction energy of -SH group or disulfide group with neighboring PG-1 monomers. For example, A indicates the interaction energy of SH or –S–S– group in monomer A with neighboring monomers in the barrel, B and H. Similarly, B indicates the interaction energy of SH or –S–S– group in monomer B with neighboring monomers A and C, and so on

	A	B	C	D	E	F	G	H
w/o disulfide bonds								
Interaction energy	−4.68	−11.77	−5.59	−6.35	−3.96	−11.56	−4.65	−9.85
SD	2.00	3.43	2.00	2.50	1.15	3.14	2.03	3.87
With disulfide bonds								
Interaction energy	−3.40	−8.86	−4.72	−4.47	−4.63	−10.08	−3.45	−9.06
SD	1.17	2.74	2.22	1.49	1.31	3.63	1.22	2.67

SUVs, mostly entropy-dominated (Gottler et al. 2008). These results are very close to the -7.8 kcal/mol measured here for 75:POPC/25:POPG LUVs. A recent ITC study found strong, exothermic interaction of PG-1 with DMPC but essentially no interaction with DOPC (Henderson et al. 2019), consistent with the present observations. Gottler

et al. also found no interaction with DOPC (Gottler et al. 2008). The significant effect of membrane thickness on peptide interaction with zwitterionic bilayers suggests insertion rather than surface interaction. Binding of protegrin on the surface of zwitterionic membranes was found to be negligible according to our previous implicit membrane modeling results (Lazaridis et al. 2013).

Cooperativity in the action of antimicrobial peptides has been observed and discussed widely (Huang 2006). This work presents a new way that this cooperativity can be assessed, by adding fluorescently labeled peptides onto a background of unlabeled peptides. The result that binding becomes stronger as the concentration of peptide in the membrane increases is an indication of positive cooperativity. Cooperativity can also be inferred in ITC experiments on DMPC, where the heat released upon protegrin-membrane interaction initially increases as peptide concentration increases (Henderson et al. 2019). One possible mechanism for cooperativity could be some type of oligomerization taking place in the membrane, as has been suggested on the basis of solid-state NMR studies (Buffy et al. 2005; Mani et al. 2006) and explored by various computational studies (Jang et al. 2006; Langham et al. 2008; Prieto et al. 2014; Lipkin and Lazaridis 2017b; Lipkin et al. 2017).

A few previous studies used dye leakage to characterize PG-1′s perturbation of membranes and the size of its pores (Waring et al. 1996; Drin and Temsamani 2002; Robinson et al. 2005; Lai et al. 2006). Lai et al. (Lai et al. 2006) used leakage of 10-kDa fluorescent dextran molecules to estimate a pore radius of at least 15–20 Å, consistent with the present results. Mani et al. (Mani et al. 2006) cite data for blockage of PG-1 pores in the E. Coli inner membrane by polyethylene glycol of different hydrodynamic radii that suggest a maximum radius of 10.5 Å, smaller than the dextran data suggest. Determining a precise size of PG-1 pores on the basis of such experiments is difficult. The Stokes radii of FD4 and FD20 are 14 Å and 33 Å, respectively. The fact that at moderate peptide concentrations, FD4 passes and FD20 does not might seem to suggest that the pore size formed by PG-1 must have a radius of at least 14 Å, but smaller than 33 Å. However, dextrans are flexible and deformable polymers of nonspherical shape (Bohrer et al. 1979). Thus, they may be able to pass through pores smaller than what their Stokes radius suggests (Venturoli and Rippe 2005). Experiments with spherical globular proteins might provide more precise data for the pore size (Venturoli and Rippe 2005).

A number of studies examined the effect of disulfide bonds on protegrin properties by mutating the Cys, deleting the Cys, modifying the Cys thiols, or using reducing conditions. The results have been wide-ranging. Mutations of all Cys to Ala abolish antimicrobial activity (Harwig et al. 1996) and the ability to translocate into vesicle (Drin and Temsamani 2002), while the presence of at least one disulfide bond maintains activity (Cho et al. 1998). Mutating Cys to Ser also led to substantial lowering of activity (Paredes-Gamero et al. 2012). Mutation of the Cys to beta sheet-stabilizing residues along with other changes that stabilize a β-hairpin maintains activity (Lai et al. 2002). A Cys-deleted variant of PG-1 was found to adopt a β-hairpin structure in complex with LPS and maintain antimicrobial and membrane permeabilizing activity, albeit lower than PG-1 (Mohanram and Bhattacharjya 2014). Reducing conditions or modification of the thiols maintain activity (Mangoni et al. 1996; Dawson and Liu 2010), although the disulfide bonds were found necessary for ion channel formation in electrophysiology experiments (Mangoni et al. 1996). Antimicrobial activity trends are sometimes strikingly different for different species (Mangoni et al. 1996), which highlights the complexity of the bacterial killing process. Apparently, different approaches for removing the disulfides can lead to different results. The results of the present study, which uses reducing conditions, are consistent with analogous past experiments (Mangoni et al. 1996; Dawson and Liu 2010).

The simulations offer some insight into the reasons for the lack of an effect of the disulfide bonds. The aqueous simulation shows that a peptide with reduced disulfide bonds makes a stable β-hairpin, although different from the native one. Interaction energy analysis shows that the reduced Cys experience significant stabilizing interactions within a monomer and with neighboring monomers. These interactions would be absent in a mutation to Ala or Ser, which may explain the different results obtained by mutation. A sheared β-barrel also appears stable without the disulfide bonds, although in a slightly different configuration. The size of the pores formed by these sheared β-barrels is similar to the smaller pores identified by the present experiments that only allow free dye leakage. Previous simulations of a C → Y mutant found a stable but more flexible β-hairpin, at least up to 70 ns (Castro et al. 2008). A recent study found problems with three force fields (other than Charmm 36 used here) in maintaining stable protegrin-like β-hairpins (Deplazes et al. 2020). No such problems are apparent in our simulations. The combination of the experimental and computational results presented here will be used as a basis for designing future studies linking structural and functional aspects of protegrin-bilayer interactions.

Acknowledgements This work was supported by the NIH (GM117146). Anton 2 computer time was provided by the Pittsburgh Supercomputing Center (PSC) through Grant R01GM116961 from the National Institutes of Health. The Anton 2 machine at PSC was generously made available by D.E. Shaw Research, and computer time was provided by the National Center for Multiscale Modeling of Biological Systems through Grant No. P41GM103712-S1 from the National Institutes of Health and PSC.

References

Aumelas A, Mangoni M, Roumestand C et al (1996) Synthesis and solution structure of the antimicrobial peptide protegrin-1. Eur J Biochem 237:575–583

Bohrer MP, Deen WM, Robertson CR et al (1979) Influence of molecular configuration on the passage of macromolecules across the glomerular capillary wall. J Gen Physiol 74:583–593. https://doi.org/10.1085/jgp.74.5.583

Bolintineanu DS, Kaznessis YN (2011) Computational studies of protegrin antimicrobial peptides: a review. Peptides 32:188–201. https://doi.org/10.1016/J.Peptides.2010.10.006

Buffy JJ, Waring AJ, Hong M (2005) Determination of peptide oligomerization in lipid bilayers using 19F spin diffusion NMR. J Am Chem Soc 127:4477–4483

Castro JRM, Fuzo CA, Degrève L, Caliri A (2008) The role of disulfide bridges in the 3-D structures of the antimicrobial peptides gomesin and protegrin-1: a molecular dynamics study. Genet Mol Res 7:1070–1088. https://doi.org/10.4238/vol7-4gmr507

Cho Y, Turner JS, Dinh NN, Lehrer RI (1998) Activity of protegrins against yeast-phase *Candida albicans*. Infect Immun 66:2486–2493. https://doi.org/10.1128/iai.66.6.2486-2493.1998

Dawson RM, Liu CQ (2010) Disulphide bonds of the peptide protegrin-1 are not essential for antimicrobial activity and haemolytic activity. Int J Antimicrob Agents 36:579–580. https://doi.org/10.1016/J.Ijantimicag.2010.08.011

Deplazes E, Chin YKY, King GF, Mancera RL (2020) The unusual conformation of cross-strand disulfide bonds is critical to the stability of β-hairpin peptides. Proteins Struct Funct Bioinforma 88:485–502. https://doi.org/10.1002/prot.25828

Drin G, Temsamani J (2002) Translocation of protegrin I through phospholipid membranes: role of peptide folding. Biochim Biophys Acta 1559:160–170. https://doi.org/10.1016/S0005-2736(01)00447-3

Fahrner RL, Dieckmann T, Harwig SSL et al (1996) Solution structure of protegrin-1, a broad-spectrum antimicrobial peptide from porcine leukocytes. Chem Biol 3:543–550

Gottler LM, Bea RDLS, Shelburne CE et al (2008) Using fluorous amino acids to probe the effects of changing hydrophobicity on the physical and biological properties of the β-hairpin antimicrobial peptide protegrin-1. Biochemistry 47:9243–9250. https://doi.org/10.1021/bi801045n

Harwig SSL, Waring A, Yang HJ et al (1996) Intramolecular disulfide bonds enhance the antimicrobial and lytic activities of protegrins at physiological sodium chloride concentrations. Eur J Biochem 240:352–357

Heller WT, Waring AJ, Lehrer RI, Huang HW (1998) Multiple states of beta-sheet peptide protegrin in lipid bilayers. Biochemistry 37:17331–17338

Henderson JM, Iyengar NS, Lam KLH et al (2019) Beyond electrostatics: antimicrobial peptide selectivity and the influence of cholesterol-mediated fluidity and lipid chain length on protegrin-1 activity. Biochim Biophys Acta. https://doi.org/10.1016/j.bbamem.2019.04.011

Henderson JM, Waring AJ, Separovic F, Lee KYC (2016) Antimicrobial peptides share a common interaction driven by membrane line tension reduction. Biophys J 111:2176–2189. https://doi.org/10.1016/j.bpj.2016.10.003

Huang HW (2006) Molecular mechanism of antimicrobial peptides: the origin of cooperativity. Biochim Biophys Acta 1758:1292–1302. https://doi.org/10.1016/J.Bbamem.2006.02.001

Huang J, Mackerell AD (2013) CHARMM36 all-atom additive protein force field: validation based on comparison to NMR data. J Comput Chem 34:2135–2145. https://doi.org/10.1002/jcc.23354

Jang H, Ma B, Woolf TB, Nussinov R (2006) Interaction of protegrin-1 with lipid bilayers: membrane thinning effect. Biophys J 91:2848–2859. https://doi.org/10.1529/Biophysj.106.084046

Kokryakov VN, Harwig SSL, Panyutich EA et al (1993) Protegrins-leukocyte antimicrobial peptides that combine features of corticostatic defensins and tachyplesins. FEBS Lett 327:231–236

Ladokhin AS, Selsted ME, White SH (1997) Sizing membrane pores in lipid vesicles by leakage of co-encapsulated markers: pore formation by melittin. Biophys J 72:1762–1766

Lai JR, Epand RF, Weisblum B et al (2006) Roles of salt and conformation in the biological and physicochemical behavior of protegrin-1 and designed analogues: correlation of antimicrobial, hemolytic, and lipid bilayer-perturbing activities. Biochemistry 45:15718–15730. https://doi.org/10.1021/Bi0617759

Lai JR, Huck BR, Weisblum B, Gellman SH (2002) Design of non-cysteine-containing antimicrobial beta-hairpins: structure-activity relationship studies with linear protegrin-1 analogues. Biochemistry 41:12835–12842

Lam KLH, Wang H, Siaw TA et al (2012) Mechanism of structural transformations induced by antimicrobial peptides in lipid membranes. Biochim Biophys Acta 1818:194–204. https://doi.org/10.1016/J.Bbamem.2011.11.002

Langham AA, Ahmad AS, Kaznessis YN (2008) On the nature of antimicrobial activity: a model for protegrin-1 pores. J Am Chem Soc 130:4338–4346. https://doi.org/10.1021/Ja0780380

Lazaridis T, He Y, Prieto L (2013) Membrane interactions and pore formation by the antimicrobial peptide protegrin. Biophys J 104:633–642. https://doi.org/10.1016/J.Bpj.2012.12.038

Lipkin R, Lazaridis T (2017a) Computational studies of peptide-induced membrane pore formation. Philos Trans B 372:20160219. https://doi.org/10.1098/rstb.2016.0219

Lipkin R, Lazaridis T (2017b) Computational prediction of the optimal oligomeric state for membrane-inserted β -barrels of protegrin-1 and related mutants. J Pept Sci 23:334–345. https://doi.org/10.1002/psc.2992

Lipkin R, Pino-Angeles A, Lazaridis T (2017) Transmembrane pore structures of β-hairpin antimicrobial peptides by all-atom simulations. J Phys Chem B 121:9126–9140. https://doi.org/10.1021/acs.jpcb.7b06591

Lipkin RB, Lazaridis T (2015) Implicit membrane investigation of the stability of antimicrobial peptide β-barrels and arcs. J Membr Biol 248:469–486

Mangoni ME, Aumelas A, Charnet P et al (1996) Change in membrane permeability induced by protegrin 1: implication of disulphide bridges for pore formation. FEBS Lett 383:93–98

Mani R, Cady SD, Tang M et al (2006) Membrane-dependent oligomeric structure and pore formation of beta-hairpin antimicrobial peptide in lipid bilayers from solid-state NMR. Proc Natl Acad Sci USA 103:16242–16247

Mohanram H, Bhattacharjya S (2014) Cysteine deleted protegrin-1 (CDP-1): anti-bacterial activity, outer-membrane disruption and selectivity. Biochim Biophys Acta 1840:3006–3016. https://doi.org/10.1016/j.bbagen.2014.06.018

Montgomery DC, Peck EA (1982) Introduction to linear regression analysis. Wiley, New York

Paredes-Gamero EJ, Martins MNC, Cappabianco FAM et al (2012) Characterization of dual effects induced by antimicrobial peptides: regulated cell death or membrane disruption. Biochim Biophys Acta 1820:1062–1072. https://doi.org/10.1016/j.bbagen.2012.02.015

Phillips JC, Braun R, Wang W et al (2005) Scalable molecular dynamics with NAMD. J Comput Chem 26:1781–1802. https://doi.org/10.1002/Jcc.20289

Prieto L, He Y, Lazaridis T (2014) Protein arcs may form stable pores in lipid membranes. Biophys J 106:154–161. https://doi.org/10.1002/prot.22866

Robinson JA, Shankaramma SC, Jettera P et al (2005) Properties and structure-activity studies of cyclic beta-hairpin peptidomimetics based on the cationic antimicrobial peptide protegrin I. Bioorg Med Chem 13:2055–2064. https://doi.org/10.1016/J.Bmc.2005.01.009

Rui H, Lee J, Im W (2009) Comparative molecular dynamics simulation studies of protegrin-1 monomer and dimer in two different lipid bilayers. Biophys J 97:787–795. https://doi.org/10.1016/J.Bpj.2009.05.029

Rui HA, Im W (2010) Protegrin-1 orientation and physicochemical properties in membrane bilayers studied by potential of mean force calculations. J Comput Chem 31:2859–2867. https://doi.org/10.1002/jcc.21580

Shaw DE, Grossman JP, Bank JA et al (2014) Anton 2: raising the bar for performance and programmability in a special-purpose molecular dynamics supercomputer. Int Conf High Perform Comput Netwk Storage Anal SC 2015:41–53. https://doi.org/10.1109/SC.2014.9

Tang M, Hong M (2009) Structure and mechanism of beta-hairpin antimicrobial peptides in lipid bilayers from solid-state NMR spectroscopy. Mol Biosyst 5:317–322. https://doi.org/10.1039/B820398a

Usachev KS, Klochkova SVEOAKEA (2015) Antimicrobial peptide protegrin-3 adopt an antiparallel dimer in the presence of DPC micelles: a high-resolution NMR study. J Biomol NMR 62:71–79. https://doi.org/10.1007/s10858-015-9920-0

Usachev KS, Kolosova OA, Klochkova EA et al (2017) Oligomerization of the antimicrobial peptide Protegrin-5 in a membrane-mimicking environment Structural studies by high-resolution NMR spectroscopy. Eur Biophys J 46:293–300. https://doi.org/10.1007/s00249-016-1167-5

Venturoli D, Rippe B (2005) Ficoll and dextran vs. globular proteins as probes for testing glomerular permselectivity: effects of molecular size, shape, charge, and deformability. Am J Physiol 288:605–613. https://doi.org/10.1152/ajprenal.00171.2004

Vivcharuk V, Kaznessis Y (2010) Free energy profile of the interaction between a monomer or a dimer of protegrin-1 in a specific binding orientation and a model lipid bilayer. J Phys Chem B 114:2790–2797. https://doi.org/10.1021/Jp909640g

Waring AJ, Harwig SSL, Lehrer RI (1996) Structure and activity of protegrin-1 in model lipid membranes. Protein Pept Lett 3:177–184

White SH, Wimley WC, Ladokhin AS, Hristova K (1998) Protein folding in membranes: determining energetics of peptide-bilayer interactions. Methods Enzymol 295:62–87

Wimley WC, Selsted ME, White SH (1994) Interactions between human defensins and lipid bilayers: evidence for formation of multimeric pores. Protein Sci 3:1362–1373

Yamaguchi S, Hong T, Waring A et al (2002) Solid-state NMR investigations of peptide-lipid interaction and orientation of a beta-sheet antimicrobial peptide, protegrin. Biochemistry 41:9852–9862

Yang L, Weiss TM, Lehrer RI, Huang HW (2000) Crystallization of antimicrobial pores in membranes: magainin and protegrin. Biophys J 79:2002–2009